
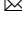










APOBEC3-dependent kataegis and TREX1-driven chromothripsis during telomere crisis

John Maciejowski^{1,2,6}  , Aikaterini Chatzipli^{3,6}, Alexandra Dananberg¹, Kevan Chu¹, Eleonore Toufektchan¹, Leszek J. Klimczak^{1,4} , Dmitry A. Gordenin⁵ , Peter J. Campbell³   and Titia de Lange²  

Chromothripsis and kataegis are frequently observed in cancer and may arise from telomere crisis, a period of genome instability during tumorigenesis when depletion of the telomere reserve generates unstable dicentric chromosomes^{1–5}. Here we examine the mechanism underlying chromothripsis and kataegis by using an in vitro telomere crisis model. We show that the cytoplasmic exonuclease TREX1, which promotes the resolution of dicentric chromosomes⁴, plays a prominent role in chromothriptic fragmentation. In the absence of TREX1, the genome alterations induced by telomere crisis primarily involve breakage–fusion–bridge cycles and simple genome rearrangements rather than chromothripsis. Furthermore, we show that the kataegis observed at chromothriptic breakpoints is the consequence of cytosine deamination by APOBEC3B. These data reveal that chromothripsis and kataegis arise from a combination of nucleolytic processing by TREX1 and cytosine editing by APOBEC3B.

To model telomere crisis, we used a previously established model system based on RPE1 cells wherein the Rb and p53 pathways are disabled with short hairpin RNAs and telomere fusions are generated with a doxycycline-inducible dominant negative allele of the shelterin protein TRF2 (refs. ^{4,6}). The resulting dicentric chromosomes persist through mitosis to form long (50–200 μ m) DNA bridges that are generally resolved before the connected daughter cells enter the next S phase. Bridge resolution is accelerated by the exonucleolytic activity of TREX1, which accumulates on the DNA bridge after nuclear envelope rupture and generates replication protein A (RPA)-coated single-stranded DNA (ssDNA)^{4,7–9}. Rearranged clonal cell lines isolated after progression through this in vitro telomere crisis showed frequent chromothripsis in a pattern similar to that in cancer: the chromothripsis events were limited to (parts of) chromosome arms rather than involving whole chromosomes^{4,10}. Furthermore, as is the case for chromothripsis in cancer, the breakpoints showed kataegis with the hallmarks of APOBEC3 editing^{4,11,12}.

To determine whether TREX1 contributes to chromothripsis after telomere crisis, TREX1-deficient cell lines generated by CRISPR–Cas9 editing (hereafter *TREX1* knockouts) were subjected to telomere crisis alongside the TREX1-proficient T2p1 cell line and clonal postcrisis descendants were isolated for whole-genome sequencing (WGS). Since only some clones are expected to have experienced telomere crisis¹, initial identification of clones with

genomic alterations was necessary. To determine whether low-pass WGS can identify relevant copy number (CN) changes evident at higher coverages, 17 postcrisis clones derived from T2p1 were analyzed at both 1 \times and 30 \times sequence coverage (Fig. 1a–d)^{13,14}. Among chromosomes showing no CN changes in 1 \times WGS analysis, 67% also did not show CN changes in high-coverage WGS and 30% showed 1–3 CN changes (hereafter referred to as simple events) (Fig. 1b). Only 3% of chromosomes lacking evidence for CN changes in 1 \times WGS contained ≥ 4 CN changes (hereafter referred to as complex events) in 30 \times WGS (Fig. 1b). Of 37 chromosomes showing 1–3 CN changes in 1 \times WGS, 19 contained >3 CN changes in 30 \times WGS (Fig. 1b). The discrepancy in the segments missed by 1 \times WGS but reported in the 30 \times data is probably due to the conservative thresholds for calling gains and losses in low-coverage data. Overall, the 1 \times analysis had an acceptable false negative rate of $<10\%$ (32 of 391 chromosomes) with regard to identifying chromosomes with complex events. Similarly, the false positive rate of the 1 \times coverage analysis was well below 10% since only 1 out of 19 chromosomes with complex events detected in 1 \times WGS did not show ≥ 4 CN in the 30 \times coverage. These data indicated that 1 \times WGS allows the identification of informative postcrisis clones.

Comparison of the 1 \times WGS data obtained from 417 *TREX1* knockout postcrisis clones with 117 T2p1 clones showed that among clones with CN changes, the frequency of complex events was lower in the *TREX1* knockout setting both with regard to clones containing complex events and the proportion of chromosomes showing complex events (Fig. 1c–e and Extended Data Fig. 1a). Furthermore, the number of CN changes associated with complex events was lower in the *TREX1* knockout setting (Fig. 1e). These results indicate that cells progressing through telomere crisis without TREX1 sustain fewer complex chromosome rearrangements. We considered that the diminished incidence of complex rearrangements in the *TREX1* knockout clones might be due to altered survival after telomere crisis, creating a bias in the analysis. However, *TREX1* knockout cells treated with doxycycline showed the same frequency of cell death (5–10%) as doxycycline-treated cells with TREX1 (Extended Data Fig. 1b). Furthermore, in one telomere crisis induction experiment, we compared the plating efficiency of the *TREX1* knockout and T2p1 cells and found that the *TREX1* knockout cells formed colonies at approximately 25% lower frequency than the T2p1 cells (Extended Data Fig. 1c). In this experiment, the frequency of complex rearrangements in the resulting *TREX1* knockout clones was

¹Molecular Biology Program, Sloan Kettering Institute, Memorial Sloan Kettering Cancer Center, New York, NY, USA. ²Laboratory for Cell Biology and Genetics, The Rockefeller University, New York, NY, USA. ³Wellcome Sanger Institute, Wellcome Sanger Institute Campus, Hinxton, UK. ⁴Integrative Bioinformatics Support Group, NIEHS, Research Triangle Park, NC, USA. ⁵Genome Integrity and Structural Biology Laboratory, NIEHS, Research Triangle Park, NC, USA. ⁶These authors contributed equally: John Maciejowski, Aikaterini Chatzipli.  e-mail: maciej@mskcc.org; pc8@sanger.ac.uk; delange@rockefeller.edu

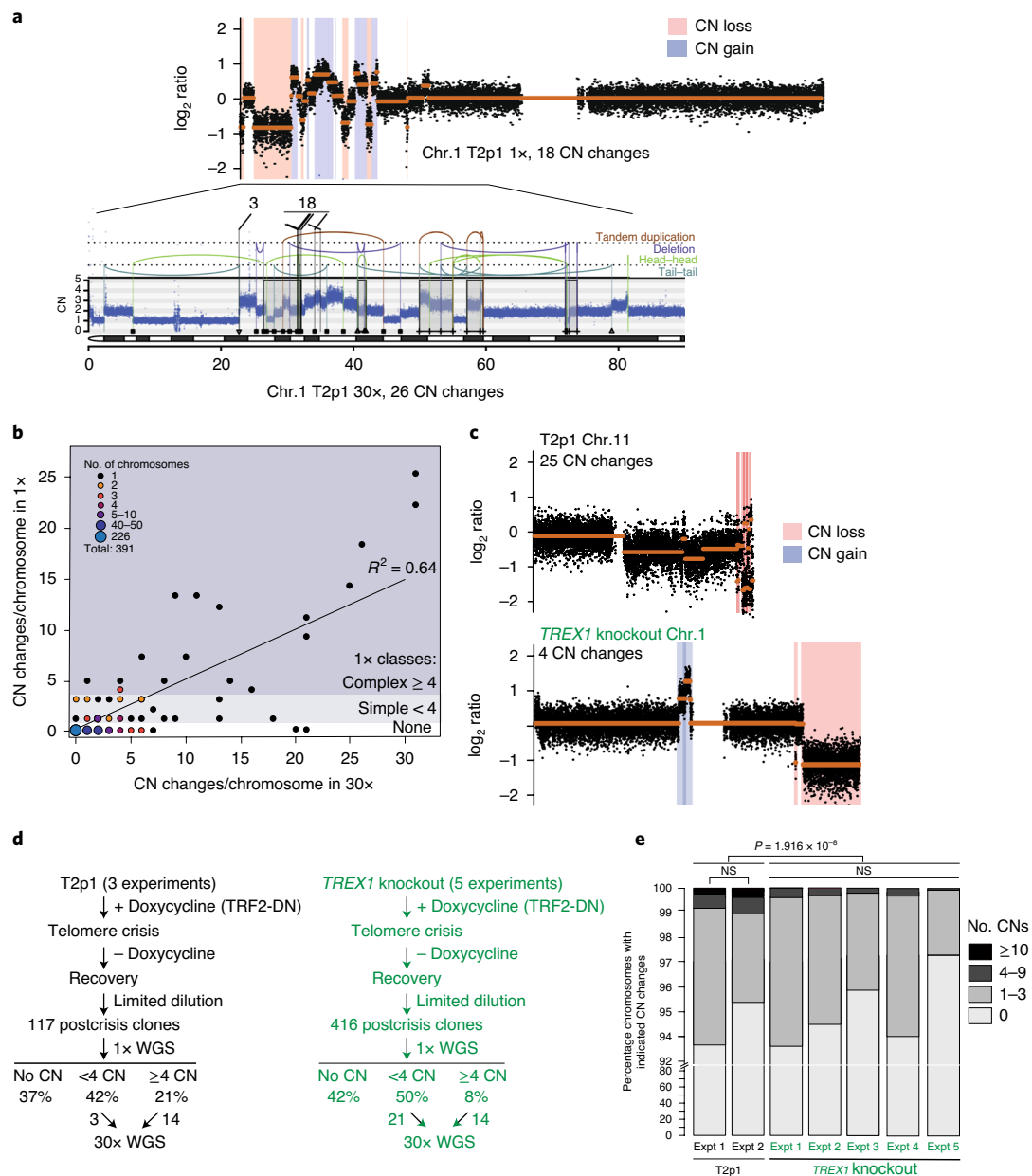


Fig. 1 | The effect of TREX1 on telomere-crisis-induced rearrangements. a, Example of comparison of 1x and 30x WGS analysis of part of chromosome 1 in a clone derived from T2p1 cells induced to undergo telomere crisis. Top: QDNAseq analysis of 1x target coverage genomic sequencing data. Regions of CN loss (pink highlight) and gain (blue highlight) are indicated. CN profiles were log₂-transformed. Bottom: DNA CN profile (estimated CN over genomic windows) and rearrangement joins obtained from Battenberg analysis of 30x target coverage genomic sequencing data. The colored arcs represent joins with the type of rearrangement and orientation as identified on the right. Rearrangement joins are further classified into discrete events as indicated by triangles, squares and plus symbols (see Methods). Interchromosomal rearrangements junctions linking to chromosomes 3 and 18 are indicated. **b**, Comparison of detection of DNA CN changes per chromosome in 1x and 30x WGS of 391 chromosomes from postcrisis T2p1 clones. The size and color of the dots highlight the approximate number of chromosomes with the indicated CN changes detected in 1x and 30x WGS. No events, simple events and complex events are defined on the right. **c**, Examples of DNA CN profiles (1x(QDNAseq)) of a T2p1 and a TREX1 knockout postcrisis clone. **d**, Analysis pipeline and summary of the number of postcrisis T2p1 and TREX1 knockout clones isolated from $n = 5$ independent telomere crisis experiments, the frequency of simple and complex CN changes detected (1x) and the number of clones selected for 30x WGS. **e**, Stacked bar plot of chromosomes from T2p1 and TREX1 knockout postcrisis clones. Data derived from 1x WGS of 117 subclones (2,691 chromosomes) and 301 subclones (6,923 chromosomes) from T2p1 and TREX1 knockout clones, respectively. P values were derived from a chi-squared test for trend in proportions. NS, not significant.

7%, whereas the T2p1 clones showed a frequency of 25% (Extended Data Fig. 1a). We also noted that T2p1 and derivative cell lines are unlikely to perish due to cyclic GMP-AMP synthase (cGAS)-stimulator of interferon genes (STING) signaling in response to

genome instability, since their cGAS expression level is too low to be detected by western blotting (Extended Data Fig. 1d) (ref. ¹⁵). Additionally, DNA bridges did not elicit cGAS-STING signaling in an analogous model of telomere crisis in cGAS⁺ MCF10A cells¹⁶.

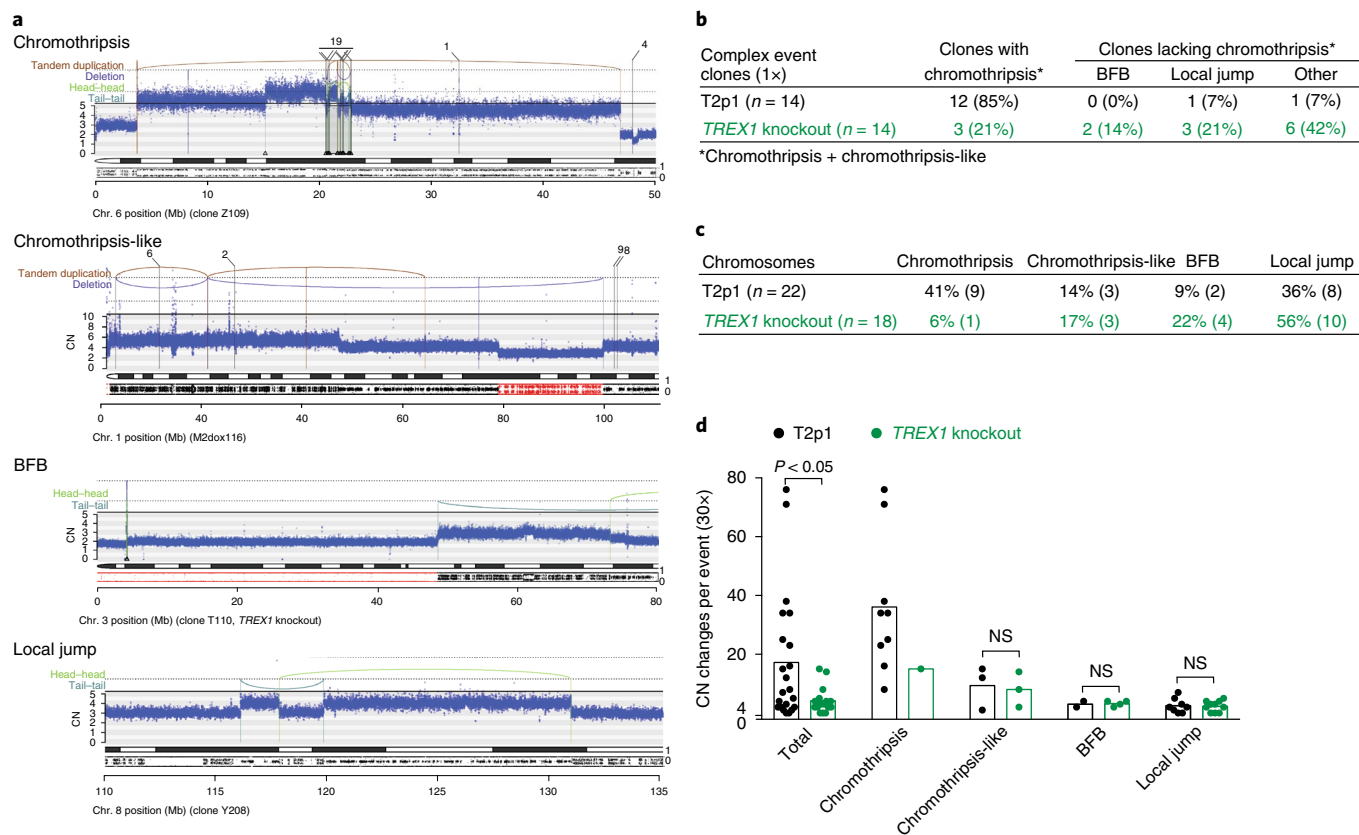


Fig. 2 | TREX1 promotes chromothripsis. **a**, Examples of chromothripsis (see also Figs. 1a and 3h,i), chromothripsis-like, BFB and local jump patterns in postcrisis clones derived from T2p1 and *TREX1* knockout cells. DNA CN profiles and rearrangement joins were obtained from 30x target coverage WGS. Annotation as in Fig. 1a. Variant allele frequency tracks are shown below the chromosome ideograms. **b**, Summary of the number of clones that displayed the types of rearrangements shown in **a** as determined by 30x WGS of 14 T2p1 and *TREX1* knockout postcrisis clones with complex events observed in 1x WGS. **c**, Summary of the number of chromosomes in postcrisis T2p1 and *TREX1* knockout clones examined in **b** that display the indicated rearrangements. **d**, Plot of the number of CN changes associated with the complex events indicated in postcrisis T2p1 and *TREX1* knockout clones described in **b**. *P* values derived from an analysis of variance. Statistical testing of CN differences in chromothripsis events between T2p1 and *TREX1* knockouts was not possible because the dataset only includes one chromothripsis event in the *TREX1* knockouts.

Nonetheless, we cannot fully rule out a difference in the survival of the *TREX1* knockout clones that may affect the frequency of observed rearrangements.

Postcrisis clones were screened for CN changes at 1x and those with a minimum of 4 CN changes (complex) on at least 1 chromosome qualified as candidates for sequencing at high coverage (Fig. 1d and Extended Data Fig. 1a). From these candidate clones, an equal number (14) of T2p1 and *TREX1* knockout clones were selected for 30x WGS analysis. In addition, some clones with simple events were selected for sequencing at 30x resulting in a total of 17 and 35 clones for T2p1 and *TREX1* knockout, respectively (Fig. 1d and Extended Data Fig. 1a).

The genomic alterations observed using 30x analysis in these clones were grouped into 4 categories (Fig. 2a): chromothripsis (as defined elsewhere¹⁷); chromothripsis-like, which we define in the present study as a chromothripsis pattern with <10 structural variants (see Methods); breakage–fusion–bridge (BFB) cycles (as defined elsewhere^{18,19}); and a fourth category referred to as local jumps. Local jumps comprise two broad patterns: a cluster of 2–5 local rearrangements, often with low-amplitude CN gains and breakpoints in an inverted orientation, thought to arise from replication-based mechanisms; and unbalanced translocations or large deletions with a locally derived fragment inserted at the breakpoint²⁰.

Of the 14 selected T2p1 postcrisis clones with ≥ 4 CN changes in 1x coverage analysis (Fig. 1e and Extended Data Fig. 1a), 12 (86%)

had either chromothripsis or a chromothripsis-like pattern on 30x WGS (Fig. 2b,c). Consistent with telomere dysfunction-derived events, chromothripsis was often localized to distal parts of chromosome arms (Extended Data Fig. 2). In contrast, among the 14 *TREX1* knockout clones with complex events analyzed by 30x WGS, only 3 (21%) showed chromothripsis or chromothripsis-like patterns (Fig. 2b,c). Taken together with the low-coverage data, these data indicate that chromothripsis is more frequent when cells experience telomere crisis in the presence of *TREX1*.

The patterns of structural variation in the postcrisis *TREX1* knockout clones showed that other abnormalities emerge instead of chromothripsis (Fig. 2c). Whereas the majority (57%) of CN changes in the T2p1 clones were classified as chromothripsis or chromothripsis-like, *TREX1* knockout clones predominantly showed BFB and local jump signatures (Fig. 2c,d and Extended Data Fig. 3). Commensurate with this, the number of CN changes per event was lower in the *TREX1* knockout clones than in the T2p1 clones (Fig. 2d). The implication of these data is that *TREX1* knockout cells resolve DNA bridges formed in telomere crisis through simple structural events rather than chromothripsis.

Some of the clones showed evidence of parallel or sequential telomere crises with chromothripsis. Parallel crises manifested as chromothripsis affecting two separate regions where virtually all the rearrangements were confined to within each region, suggesting that the damage and repair were isolated from one another, either in time or space. Sometimes the two regions were linked

by a single translocation, which presumably occurred after the chromothripsis resolved, stabilizing the two derivative chromosomes (Extended Data Fig. 4). In other clones, we found evidence for sequential events affecting the same derivative chromosome—these manifested as separate clusters of breakpoints, one of which demarcated clonal CN changes and one demarcated subclonal CN changes (Extended Data Fig. 4). These occasional clones suggest that telomere crisis and chromothripsis are not always resolved in a single cell cycle.

Chromothripsis after telomere crisis is accompanied by kataegis with the hallmark of APOBEC3 cytosine deaminase editing: clustered and strand-coordinated mutations in cytosine residues in TCA or TCT triplets^{4,21}. The ssDNA substrate of APOBEC3 enzymes is formed by TREX1-dependent nucleolytic degradation of the DNA bridges formed in telomere crisis. Based on imaging of mTurquoise2-tagged RPA70 after TRF2-DN-induced telomere fusions (Fig. 3a–c), the ssDNA remnant of resolved DNA bridges appeared to either join the primary nucleus or remain outside the nucleus during the interphase. In the next mitosis, RPA foci were still detectable and were often incorporated into one of the daughter nuclei. In the vast majority of cases (47 out of 49 nuclei analyzed), large RPA foci remained detectable for at least 19 h, suggesting that the ssDNA APOBEC3 substrate persists for a long period after DNA bridge resolution.

Transcript analysis showed that RPE1 cells expressed *APOBEC3B* but not *ABOEC3A* (Fig. 3d and Extended Data Fig. 5a). The *APOBEC3B* messenger RNA levels in T2p1 cells were slightly increased compared to the parental RPE1 cell line but not further induced by telomere damage (Fig. 3d). The *APOBEC3B* locus was targeted by CRISPR–Cas9 editing (Extended Data Fig. 5) and loss of *APOBEC3B* expression was verified by immunoblotting (Fig. 3e and Extended Data Fig. 5f). Cytosine deaminase activity in cell extracts became undetectable in *APOBEC3B* knockout cells (Fig. 3f), indicating that the APOBEC3B is the major cytosine deaminase in the telomere crisis cell line. The absence of APOBEC3B did not affect the resolution of the DNA bridges formed by dicentric chromosomes (Fig. 3g).

The pipeline of the 1× and 30× WGS analysis described earlier was applied to 375 clones derived from 4 independent experiments performed with 2 independent *APOBEC3B* knockout cell lines (Extended Data Fig. 6a–c). The percentage of postcrisis clones showing CN changes detectable by 1× WGS and the frequency of clones with either simple or complex events was similar in the absence and presence of APOBEC3B (Extended Data Fig. 6a). Furthermore, 30× WGS of 23 selected clones showed that the prevalence of chromothripsis and chromothripsis-like events was not affected by the absence of APOBEC3B (Fig. 3h,i and Extended Data Fig. 6b,c).

As expected, a substantial number of kataegis events involving primarily C to T changes in TCA triplets were observed in the postcrisis wild-type T2p1 clones (Fig. 3h–k). Kataegis was associated with chromothripsis; as expected, most events were located within 5 kilobases (kb) of the nearest breakpoint and many clusters contained more than 10 mutations (ranging from 12 to 181) (Fig. 3j). The spectrum of changes and the nucleotide context of the kataegis events were consistent with APOBEC3 editing (Fig. 3k,l). Interestingly, kataegis in the T2p1 clones never occurred at the simple BFB and local jump breakpoints. Since these simple rearrangements do not require TREX1 (Fig. 2), they may not involve generation of the ssDNA substrate for APOBEC3 editing. Importantly, despite their frequent chromothripsis(-like) events, the *APOBEC3B* knockout postcrisis clones showed only three kataegis events and these events had relatively few (six, seven and ten) mutations (Fig. 3j). Furthermore, the cytosine mutations observed in the *APOBEC3B* knockout clones showed minimal enrichment for APOBEC3 motifs (Fig. 3k,l). Collectively, the data provide experimental evidence for the link between APOBEC3 activity and the generation of signatures 2 and 13 in the cancer genomes²².

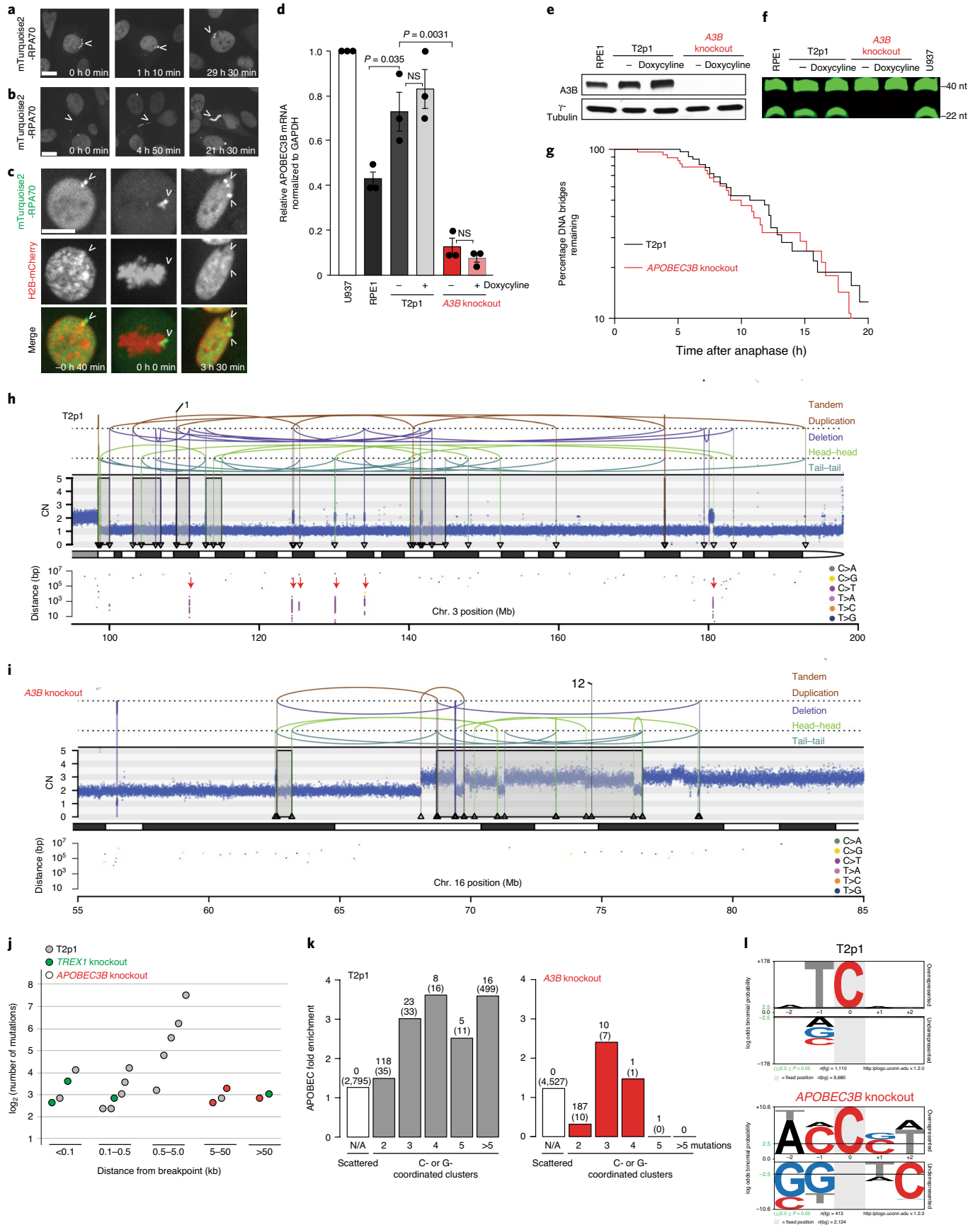
The overall frequency of chromothripsis in the *APOBEC3B* knockout and T2p1 clones was similar and distinct from the lower frequency observed in the *TREX1* knockout clones (Fig. 4a and Extended Data Fig. 6b,c). However, complex events in the *APOBEC3B* knockout clones generally showed fewer CN changes per complex event, although this fell just short of statistical significance (Fig. 4b,c). Therefore, cytosine deamination may potentially lead to strand breakage and thereby increase the DNA fragmentation underlying chromothripsis (Fig. 4e), although this strand breakage is not required for DNA bridge resolution (Fig. 3g). Following uracil glycosylation (for example, by UNG2), the abasic site in ssDNA may be cleaved by abasic endonucleases such as APE1 (ref. 23), despite its preference for double-stranded DNA. The idea that APOBEC3B could function as a cytidine-specific initiator of DNA fragmentation is consistent with the finding that APOBEC3B overexpression can induce DNA damage²⁴.

These data establish that TREX1, previously shown to promote the resolution of DNA bridges formed by dicentric chromosomes in our experimental system⁴, plays a critical role in the chromothripsis resulting from bridge resolution. Furthermore, the data presented in this study show that the kataegis accompanying this chromothripsis is largely due to cytosine deamination by APOBEC3B. While this manuscript was under review, Umbreit et al.²⁵ reported that TREX1 does not contribute to the resolution of bridges formed through telomere fusion in our T2p1 cell line. One difference between their experimental setup and ours is the much shorter induction of TRF2-DN (12 versus 72 h). A 12-h

Fig. 3 | APOBEC3B induces kataegis during telomere crisis. **a**, Still photographs from live cell imaging of T2p1 cells expressing mTurquoise2-RPA70 at the indicated time points after doxycycline treatment showing ssDNA joining the primary nucleus. **b**, As in **a** but showing an example of ssDNA remaining outside the nucleus. **c**, As in **a** but showing both H2B-mCherry and mTurquoise2-RPA70 and representing an example of ssDNA joining a daughter nucleus during mitosis (the times before and after mitosis are given). Images are representative of $n=3$ independent experiments. **d**, Normalized *APOBEC3B* mRNA levels in the indicated cell lines based on qPCR with reverse transcription and represented relative to U937 cells. The mean and s.d. of $n=3$ independent experiments are shown. P values were derived from a Student's t -test. **e**, Immunoblotting for endogenous APOBEC3B before or after 48 h of doxycycline treatment in the indicated cell lines. **f**, Cytidine deaminase activity assay in the indicated cell lines. The expected DNA fragment sizes are indicated. The gel is representative of $n=3$ independent experiments. **g**, Timing of DNA bridge resolution after anaphase in T2p1 and *APOBEC3B* knockout cells expressing H2B-mCherry and mTurquoise2-RPA70 and induced with doxycycline. Data were obtained from two independent experiments (T2p1=53, 55 DNA bridges; *APOBEC3B* knockout = 65, 67 DNA bridges). **h,i**, Examples of DNA CN profile and rearrangement joins of T2p1 (**h**) and *APOBEC3B* knockout (**i**) post-telomere crisis clones with chromothripsis obtained from 30× WGS. Annotation as in Fig. 1a. The red arrows indicate kataegis clusters. **j**, Plot of distance of cytosine mutation clusters (regardless of strand coordination) indicating the number of mutations and the distance to the nearest rearrangement breakpoint in postcrisis wild-type T2p1 clones (gray), *TREX1* knockout clones (green) and *APOBEC3B* knockout clones (red). **k**, APOBEC signature motif enrichment in C- or G-coordinated clusters of the indicated sizes and intermutational distances <10 kb (as described in the methods of ref. 27) in postcrisis T2p1 and *APOBEC3B* knockout clones. The number of clusters and (number of tCw motifs) is shown above each bar. N/A, not applicable. **l**, Statistical evaluation of nucleotide prevalence around cytosines mutated in C- or G-coordinated clusters based on data as in **k**. All scale bars, 5 μm.

induction is expected to generate very few telomere fusion events and will create bridges containing a single chromatid rather than multiple fused chromatids. It is conceivable that bridges containing

a single chromatid can be broken mechanically (as suggested by Umbreit et al.²⁵) whereas bridges containing multiple chromatids require TREX1 for their resolution. Since TREX1 localizes to



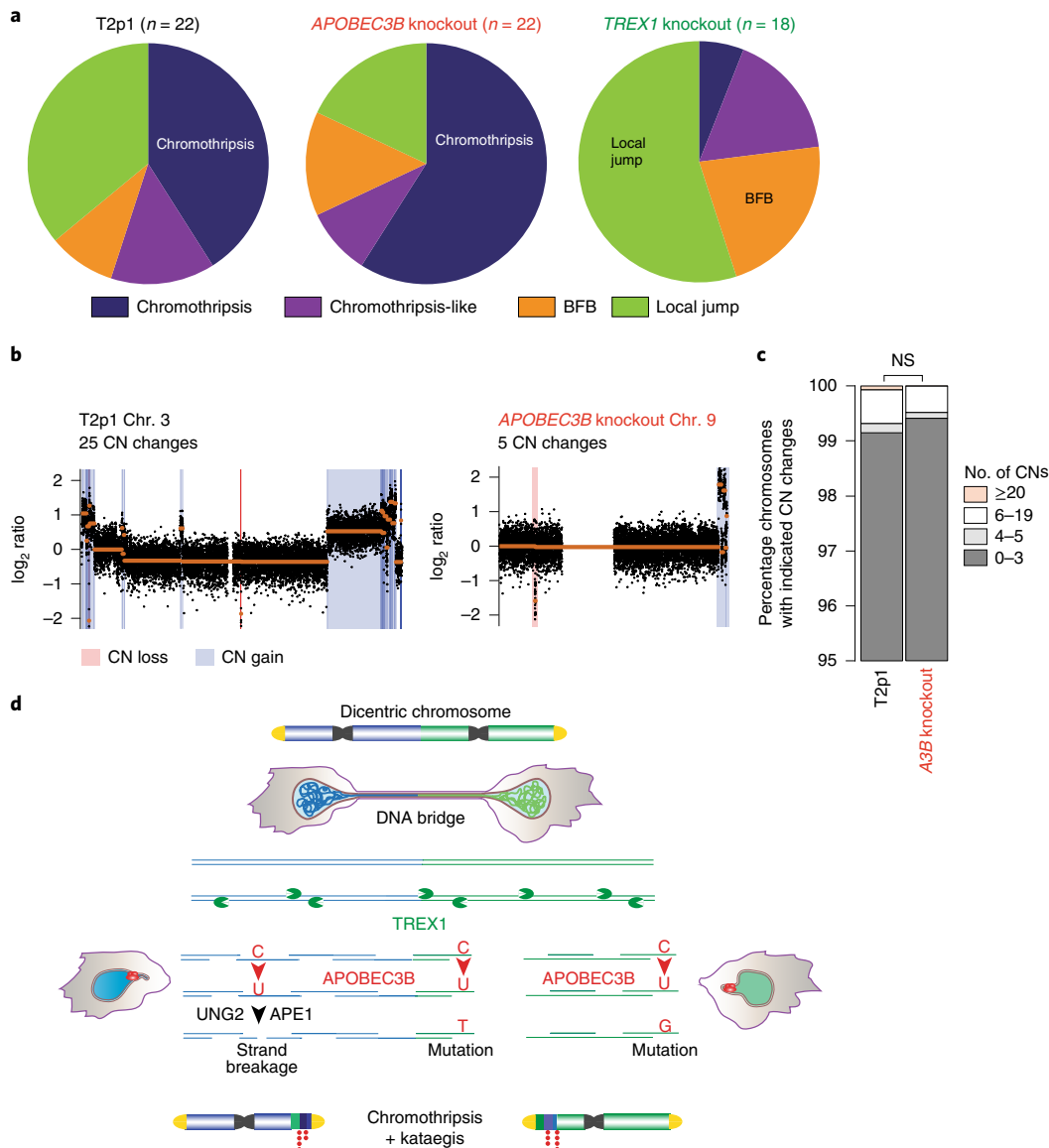


Fig. 4 | TREX1 and APOBEC3B determine genome instability during telomere crisis. **a**, Pie charts summarizing detected events in the indicated cell lines. Data obtained from 30× WGS (n = total number of chromosomes with either of the 4 types of events). **b**, Example of DNA CN profiles of T2p1 and *APOBEC3B* knockout post-telomere crisis clones from 1× WGS. **c**, Stacked bar plot of chromosomes from T2p1 and *APOBEC3B* knockout postcrisis clones. Data derived from 1× WGS of 117 subclones (2,691 chromosomes) and 375 subclones (8,675 chromosomes) from T2p1 and *APOBEC3B* knockout clones, respectively. P value was derived from a chi-squared test for trend in proportions. **d**, Schematic displaying the inferred TREX1- and APOBEC3B-dependent events leading to chromothripsis and kataegis during telomere crisis.

DNA bridges, is responsible for the formation of ssDNA and promotes bridge resolution⁴, we consider it likely that the generation of ssDNA by TREX1 underlies most chromothripsis events in this system. Furthermore, the finding of APOBEC3 editing at chromothriptic breakpoints in this and other studies^{11,26} is consistent with TREX1-induced ssDNA as an intermediate in the process of chromothripsis. We do not know the nature and frequency of the nicks that provide TREX1 with a starting point for 3' resection. In addition, it is not yet clear how this 3' exonuclease leads to resolution of the DNA bridges. One possibility is that a bridge breaks when two TREX1 nucleases meet on opposite strands (Fig. 4d). Alternatively, DNA helicases could inadvertently stimulate the dissociation of ssDNA fragments or ssDNA could undergo breakage due to physical force. We also do not know how the ssDNA fragments are converted into the double-stranded DNA

fragments that eventually are combined into the chromothripsis region. Ultimately, it will be critical to establish whether cancers with chromothripsis and kataegis actually evolved through telomere crisis.

Online content

Any methods, additional references, Nature Research reporting summaries, source data, extended data, supplementary information, acknowledgements, peer review information; details of author contributions and competing interests; and statements of data and code availability are available at <https://doi.org/10.1038/s41588-020-0667-5>.

Received: 30 March 2020; Accepted: 19 June 2020;
Published online: 27 July 2020

References

- Campbell, P. J. Telomeres and cancer: from crisis to stability to crisis to stability. *Cell* **148**, 633–635 (2012).
- Mardin, B. R. et al. A cell-based model system links chromothripsis with hyperploidy. *Mol. Syst. Biol.* **11**, 828 (2015).
- Maciejowski, J. & de Lange, T. Telomeres in cancer: tumour suppression and genome instability. *Nat. Rev. Mol. Cell Biol.* **18**, 175–186 (2017).
- Maciejowski, J., Li, Y., Bosco, N., Campbell, P. J. & de Lange, T. Chromothripsis and kataegis induced by telomere crisis. *Cell* **163**, 1641–1654 (2015).
- Cleal, K., Jones, R. E., Grimstead, J. W., Hendrickson, E. A. & Baird, D. M. Chromothripsis during telomere crisis is independent of NHEJ and consistent with a replicative origin. *Genome Res.* **29**, 737–749 (2019).
- van Steensel, B., Smogorzewska, A. & de Lange, T. TRF2 protects human telomeres from end-to-end fusions. *Cell* **92**, 401–413 (1998).
- Fouquerel, E. et al. Targeted and persistent 8-oxoguanine base damage at telomeres promotes telomere loss and crisis. *Mol. Cell* **75**, 117–130.e6 (2019).
- Xia, Y. et al. Rescue of DNA damage after constricted migration reveals a mechano-regulated threshold for cell cycle. *J. Cell Biol.* **218**, 2545–2563 (2019).
- Vietri, M. et al. Unrestrained ESCRT-III drives micronuclear catastrophe and chromosome fragmentation. *Nat. Cell Biol.* **22**, 856–867 (2020).
- Stephens, P. J. et al. Massive genomic rearrangement acquired in a single catastrophic event during cancer development. *Cell* **144**, 27–40 (2011).
- Nik-Zainal, S. et al. Mutational processes molding the genomes of 21 breast cancers. *Cell* **149**, 979–993 (2012).
- Roberts, S. A. et al. Clustered mutations in yeast and in human cancers can arise from damaged long single-strand DNA regions. *Mol. Cell* **46**, 424–435 (2012).
- Scheinin, I. et al. DNA copy number analysis of fresh and formalin-fixed specimens by shallow whole-genome sequencing with identification and exclusion of problematic regions in the genome assembly. *Genome Res.* **24**, 2022–2032 (2014).
- Nik-Zainal, S. et al. The life history of 21 breast cancers. *Cell* **149**, 994–1007 (2015).
- Nader, G. P. F. et al. Compromised nuclear envelope integrity drivers tumor cell invasion. Preprint at *bioRxiv* <https://www.biorxiv.org/content/10.1101/2020.05.22.110122v1.full> (2020).
- Mohr, L., Toufektchan, E., Chu, K. & Maciejowski, J. ER-directed TREX1 limits cGAS recognition of micronuclei. Preprint at *bioRxiv* <https://www.biorxiv.org/content/10.1101/2020.05.18.102103v1> (2020).
- Korbel, J. O. & Campbell, P. J. Criteria for inference of chromothripsis in cancer genomes. *Cell* **152**, 1226–1236 (2013).
- Bignell, G. R. et al. Architectures of somatic genomic rearrangement in human cancer amplicons at sequence-level resolution. *Genome Res.* **17**, 1296–1303 (2007).
- Rudolph, K. L., Millard, M., Bosenberg, M. W. & DePinho, R. A. Telomere dysfunction and evolution of intestinal carcinoma in mice and humans. *Nat. Genet.* **28**, 155–159 (2001).
- Li, Y. et al. Patterns of structural variation in human cancer genomes. *Nature* **578**, 112–121 (2020).
- Roberts, S. A. et al. An APOBEC cytidine deaminase mutagenesis pattern is widespread in human cancers. *Nat. Genet.* **45**, 970–976 (2013).
- Alexandrov, L. B. et al. Signatures of mutational processes in human cancer. *Nature* **500**, 415–421 (2013).
- Kavli, B., Otterlei, M., Slupphaug, G. & Krokan, H. E. Uracil in DNA: general mutagen, but normal intermediate in acquired immunity. *DNA Repair (Amst.)* **6**, 505–516 (2007).
- Burns, M. B. et al. APOBEC3B is an enzymatic source of mutation in breast cancer. *Nature* **494**, 366–370 (2013).
- Umbreit, N. T. et al. Mechanisms generating cancer genome complexity from a single cell division error. *Science* **368**, eaba0712 (2020).
- Yousif, F. et al. The origins and consequences of localized and global somatic hypermutation. Preprint at *bioRxiv* <https://www.biorxiv.org/content/10.1101/287839v2> (2018).
- Chan, K. et al. An APOBEC3A hypermutation signature is distinguishable from the signature of background mutagenesis by APOBEC3B in human cancers. *Nat. Genet.* **47**, 1067–1072 (2015).

Publisher's note Springer Nature remains neutral with regard to jurisdictional claims in published maps and institutional affiliations.

© The Author(s), under exclusive licence to Springer Nature America, Inc. 2020

Methods

Data reporting. No statistical methods were used to predetermine sample size. The experiments were not randomized and the investigators were not blinded to allocation during the experiments and outcome assessment.

Cell culture procedures and plasmids. RPE1-hTERT and U937 cells were obtained from ATCC. RPE1-hTERT cells were cultured in a 1:1 mixture of DMEM and Nutrient Mixture F12 medium (DMEM/F12; Gibco). Phoenix virus packaging cells were grown in DMEM. U937 cells were grown in Roswell Park Memorial Institute 1640 medium. All media were supplemented with 10% FCS (Gibco), 100 U ml⁻¹ penicillin/streptomycin (Thermo Fisher Scientific) and 2.5 mM L-glutamine (Thermo Fisher Scientific). T2p1 cells and their *TREX1* knockout derivatives were described previously¹. Doxycycline was used at 1 µg ml⁻¹.

Target sequence for CRISPR–Cas9-mediated gene knockouts identified by ZiFit (<http://zifit.partners.org>; see sgAPOBEC3B nos. 1 and 2 in Supplementary Table 2). Plasmids containing single guide RNAs (plasmid no. 41824; Addgene) and a human codon-optimized Cas9 (plasmid no. 41815; Addgene) were conucleofected into target cells by Nucleofector (Lonza). A total of 700,000 cells were mixed with electroporation buffer (freshly mixed 125 mM of Na₂HPO₄, 12.5 mM of KCl, 55 mM of MgCl₂, pH 7.75), 5 µg Cas9 plasmid and 5 µg guide RNA plasmid, transferred to an electroporation cuvette (BTX) and electroporated with program T23 for T2p1 cells. Cells were then allowed to recover for 48 h before a second round of electroporation. Successful CRISPR–Cas9 editing was confirmed at the polyclonal stage by mutation detection with the Surveyor nuclease assay (Transgenomic). The regions surrounding the Cas9 cut sites were PCR-amplified (using JM661, JM662, JM657 and JM658; listed in Supplementary Table 2), melted and reannealed. Reannealed PCR products were incubated with the Surveyor nuclease for 1 h at 42 °C and analyzed on a 2% agarose gel with ethidium bromide. Clones were isolated by limiting dilution and screened for *APOBEC3B* deletion by PCR. Inversions resulting from successful sgA3B no. 1 and 2 cutting were identified using the primers JM662 and JM680 (Supplementary Table 2). Deletion of the wild-type *APOBEC3B* allele was confirmed using the primers JM679 and JM680 (Supplementary Table 2). Biallelic targeting was verified by western blotting and sequencing of TOPO-cloned PCR products.

Annexin V staining was performed using the annexin V Apoptosis detection kit (BD Biosciences) according to the manufacturer's instructions.

Immunoblotting. For immunoblotting, cells were collected by trypsinization and lysed in 1× Laemmli buffer (50 mM of Tris, 10% glycerol, 2% SDS, 0.01% bromophenol blue, 2.5% β-mercaptoethanol) at 10⁷ cells per ml. Lysates were denatured at 100 °C and DNA was sheared with a 28.5-gauge insulin needle. Lysate equivalent to 10⁵ cells was resolved on 8 or 10% SDS–polyacrylamide gel electrophoresis (Thermo Fisher Scientific) and transferred to nitrocellulose membranes. Membranes were blocked in 5% milk in tris-buffered saline with 0.1% Tween 20 (TBST) and incubated with primary antibody overnight at 4 °C, washed 3 times in TBST and incubated for 1 h at room temperature with horseradish peroxidase-conjugated sheep anti-mouse or donkey anti-rabbit secondary antibodies. After three washes in TBST, membranes were rinsed in TBST and proteins were developed using enhanced chemiluminescence (Amersham).

The following primary antibodies were used: anti-APOBEC3B (rabbit monoclonal, 1:1,000; catalog no. ab184990; Abcam); anti-gamma tubulin (mouse monoclonal, 1:1,000; catalog no. ab11316; Abcam); anti-cGAS (1:1,000; catalog no. 15102; Cell Signaling Technology); and anti-STING (1:1,000; catalog no. 13647; Cell Signaling Technology).

Live cell imaging and quantitation. Live cell imaging of mCherry-H2B-marked cells was performed as described previously⁴. Chromatin bridge resolution was determined by manually tracking pairs of daughter cells. Bridge resolution was inferred to take place when the base of the bridge became slack and/or recoiled. RPA and APOBEC3B were tracked based on mTurquoise2-RPA70.

Quantitative PCR (qPCR). Random hexameric primers and avian myeloblastosis virus reverse transcriptase (Roche) were used to synthesize complementary DNA from total RNA (2.5 µg) template. cDNA levels were quantified by PCR using a Roche LightCycler 480 instrument as described elsewhere²⁸. Briefly, reactions were performed in 384-well plates with each well containing 7.5 µl 2× probe master mix (Roche), 1.25 µl of H₂O, 1.05 µl of primers (5 µM each), 0.2 µl of UPL probe (Roche) and 5 µl cDNA. Reactions were incubated at 95 °C for 10 min, then 40 cycles of 95 °C for 10 s, 58 °C for 15 s and 72 °C for 2 s. *APOBEC3A* and *APOBEC3B* qPCR was performed using the primer listed in Supplementary Table 2. Cycle threshold values were calculated using the LightCycler 480 software (v.1.3). cDNA was synthesized and qPCR was performed in triplicate for each sample.

In vitro deamination assay. Cells were lysed in 25 mM of HEPES, 5 mM of EDTA, 10% glycerol, 1 mM of dithiothreitol and protease inhibitor. Protein concentrations were equalized by cell counting before lysis. Deamination reactions were performed at 37 °C using the APOBEC3B probe (5'-IRDYE800-ATTATTATTATTATTATTTCATTATTATTATTATTATTA-3') in a 10× uracil DNA glycosylase reaction buffer consisting of 1.25 µl of RNase A (0.125 mg ml⁻¹),

1 µl of probe (0.2 pmol µl⁻¹), 16.5 µl of cleared lysate and uracil DNA glycosylase (1.25 U; New England Biolabs). Abasic site cleavage was induced by adding 100 mM of NaOH and incubation at 95 °C. Reaction products were migrated on 15% urea-Tris-borate-EDTA gels and imaged on an Odyssey CLx Imaging System (LI-COR).

X Ten sequencing and mapping. Genomic DNA sequencing libraries were synthesized on robots; cluster generation and sequencing were performed using the manufacturer's pipelines. Average sequence coverage across the samples was 37.3× (range: 23.5–47.8×). Sequencing reads were aligned to the National Center for Biotechnology Information build 37 human genome using the Burrows–Wheeler Aligner MEM algorithm v.0.7.15 (ref. ²⁹) to create a BAM file with Smith–Waterman correction with PCR duplicates removed (<http://broadinstitute.github.io/picard/>).

Mutation calling. Point mutations were called using CaVEMan v.1.11.2 (ref. ³⁰) with RPE1 as reference. A simple tandem repeat filter was applied first to remove variants observed less than 5 times or if they were seen in less than 10% of the reads. Also, a variant was considered only if observed in both forward and reverse strands. To enrich for high-confidence somatic variants, variants were further filtered by removing known constitutional polymorphisms using the following human variation databases: Ensembl GRCh37; 1000 Genomes v.2.2.2; ESP6500; and ExAC v.0.3.1.

Raw mutations were filtered using a homopolymer filter. Mutations that had a homopolymer repeat of at least six bases on either side of the mutation and where the mutated base was same as the base of the homopolymer repeat(s) were removed. A soft-clip filter was used in a similar way. Mutations where more than half of the supporting reads were soft-clipped were removed.

CN analysis. We detected DNA CN aberrations by shallow WGS at 1× (average 1.3×) using quantitative DNA sequencing (QDNAseq)¹³. The genome was divided into bins of 15 kb and the method used for callBins was 'cutoffs' for deletion = 0.5, loss = 1.2, gain = 2.5 and amplification = 10. A blacklist of CN changes repeated in the same regions in at least 10% of the samples was reported and removed from the final CN data at 1×.

All clones were initially sequenced at low coverage (1×) and CN changes were assessed using the QDNAseq algorithm. Clones were selected for deeper sequencing using one of the chromothripsis criteria¹⁷ namely the density of CN changes (or breakpoints for the 30× data) set to 4. According to this, samples with more than four CN changes (complex) per chromosome were good candidates for higher coverage sequencing. These samples were ranked for the highest number of chromosomes with more than 4 CN changes; approximately the top 10% was sequenced at 30×.

We used both ASCAT (v.4.0.1)³¹ and Battenberg (<https://github.com/cancerit/cgpBattenberg>, v.3.3.0) to extract CN data from 30× WGS. ASCAT was used assuming a ploidy of four for subclonal event identification and to enhance aberrations overall for easier data manipulation. Battenberg analysis was performed using a ploidy of two, which was consistent with the QDNAseq settings for direct comparison of the data from the two algorithms.

Event identification. Events were defined through regions with high-density rearrangement breakpoints. A minimum of 4 breakpoints spaced 2 Mb apart was identified as an event. The rest of the rules applied for the identification of events were related to the propagation of the rearrangements. When one breakpoint of a rearrangement was part of an event while the second was not because of the distance rules applied, the two breakpoints were merged into the same event. When the breakpoints of the same rearrangement belonged to different events, they were merged into one event. To graphically distinguish between different events on our plots, we annotated breakpoints of events using different shapes at the bottom tips of their breakpoints (Fig. 3e,f).

Rearrangement calling and chromothripsis. To call rearrangements, we applied the BRASS (breakpoint via assembly, v.5.4.1) algorithm, which identifies rearrangements by grouping discordant read pairs that point to the same breakpoint event (github.com/cancerit/BRASS). Postprocessing filters were applied to the output to improve specificity (blacklisted recurrent breakpoints in 10% of samples). Complex chromothripsis clusters were called according to the criteria from Korbel and Campbell¹⁷: (1) a minimum of 4 breakpoints spaced 2 Mb apart was considered a high-density event; (2) oscillating CN stages were mostly detected but nonconventional chromothripsis was also seen; (3) multiple chromosomes retained loss of heterozygosity across chromosomes; (4) 1× WGS data analysis confirmed the prevalence of rearrangements; (5) the type of fragment joins in chromothripsis should be uniformly distributed. However, the chromothripsis events involve fairly low numbers of intrachromosomal rearrangements, which would decrease power in a uniform multinomial distribution; (6) ability to walk the derivative chromosome was not an applicable rule since chromothripsis takes place on chromosomes with preceding duplication through BFBs³².

Another category of events identified during this study was chromothripsis-like events, in this study as having <10 structural variants but patterns consistent

with chromothripsis. The original description of chromothripsis relied on statistical arguments to argue that the structural variants seen in such cases must have occurred in a single catastrophic event rather than by sequential rearrangements¹⁰—these statistical arguments were later formalized into criteria for identifying chromothripsis¹⁷. Essentially, the key observation is that with simulations of sequential simple rearrangements, the overall number of observed CN states in the chromosome tends to increase roughly in a logarithmic shape as the number of rearrangements increases. When we observe only two or three CN states for a chromosome containing many tens of rearrangements, this is clearly well below the expected distribution of CN states, and we have strong statistical evidence that at least some of the rearrangements were generated in a single catastrophic shattering event. The extent of breakage and relegation during a chromothripsis event clearly exists on a spectrum. While our statistical argument satisfactorily handles the more extreme numbers of rearrangements (for example, >8–10 breakpoints in a localized region with 2–3 CN states), we observed events with approximately 4–8 rearrangements that shared the general patterns of chromothripsis—namely, 2–3 oscillating CN states, alternating retention and loss of heterozygosity, balance of inverted and noninverted rearrangements and a solution that phases all rearrangements to a single derivative chromosome. However, due to the smaller number of rearrangements, it is possible to construct theoretical sequences of simple rearrangement types such as deletions, tandem duplications and reciprocal inversions that generate the observed data²⁰. While we believe the sequential model of rearrangement is unlikely to have generated the events seen in the current study, largely because the frequency of simple structural variants in the rest of the genome of these clones is so low, we cannot formally exclude this with our usual statistical reasoning. Therefore, we have termed these events ‘chromothripsis-like’.

Finally, local jumps seen mainly in TREX1 knockout clones are defined according to a previous report²⁰. Local jumps consist of an unbalanced translocation or large deletion with a locally derived fragment inserted at the breakpoint. Local distant jumps are deletions with a distant fragment from a different chromosome inserted. Both types of rearrangement were observed and grouped under the term ‘local jump’.

Kataegis. Kataegis mutation clusters were detected according to Chan et al.²⁷ with modifications. Similarly to the identification of events, mutations spaced ≤ 2 kb apart were treated as a single mutagenic event. Groups of closely spaced mutations (at least 4 mutations) were identified, such that any pair of adjacent mutations within each group was separated by less than 2 kb. To identify clusters that were unlikely to have formed by the random distribution of mutations within a genome, we computed a P value for each group. Each group with $P \leq 1 \times 10^{-4}$ was considered a bona fide mutation cluster. A recursive approach was applied, that is, all clusters passing P value filtering were identified, even if a cluster represented a subset within a larger group that did not pass the P value filter: A3A \rightarrow CTCA or TTCA; A3B \rightarrow ATCA or GTCA. TCA enrichment was calculated and significance was assessed using Fisher’s exact test:

$$E_{TCA} = (\text{Mut}_{TCA} / \text{Con}_{TCA}) / (\text{Mut}_C / \text{Con}_C)$$

where Mut indicates mutations, C indicates cytosine, and E indicates enrichment. The enrichment of YTCA and RTCA was calculated and significance was assessed using a chi-squared test based on the expected YTCA and RTCA:

$$\text{Exp}_{YTCA} = \text{Mut}_{TCA} \times \text{Con}_{YTCA} / \text{Con}_{TCA}$$

where Con_{TCA} = TCA occurrences.

Enrichment of C \rightarrow G and C \rightarrow T mutations in the TCA context was compared to other contexts and normalized by how many times the motif occurred in the genome.

Statistical model for kataegis association with genotype. We found a statistically significant relationship when comparing *APOBEC3B* knockout to T2p1 kataegis clusters by applying the negative binomial distribution to test how kataegis clusters were related to rearrangements across genotypes. Our Poisson regression model showed that *APOBEC3B* knockout samples contained a high enough number of breakpoints expected to detect kataegis clusters. The same was not true for *TREX1* knockout samples.

Statistical analysis and reproducibility. Statistical analyses were performed using Prism v.7.0d (GraphPad Software). Descriptions of the statistical tests used are provided in the figure legends.

Reporting Summary. Further information on research design is available in the Nature Research Reporting Summary linked to this article.

Data availability

All sequencing data pertaining to this study have been deposited with the European Nucleotide Archive database under primary accession no. PRJEB23723 and secondary accession no. ERP105494. All other data supporting the findings of this study are available within the article and its supplementary information files and from the corresponding author upon reasonable request. Source data are provided with this paper.

Code availability

All code used in this study is available at the Wellcome Sanger Institute GitHub page (<https://github.com/cancerit>) or by request to the authors (A.C., P.J.C.).

References

28. Refsland, E. W. et al. Quantitative profiling of the full APOBEC3 mRNA repertoire in lymphocytes and tissues: implications for HIV-1 restriction. *Nucleic Acids Res.* **38**, 4274–4284 (2010).
29. Li, H. & Durbin, R. Fast and accurate long-read alignment with Burrows–Wheeler transform. *Bioinformatics* **26**, 589–595 (2010).
30. Jones, D. et al. cgpaVEManWrapper: simple execution of CaVEMan in order to detect somatic single nucleotide variants in NGS data. *Curr. Protoc. Bioinformatics* **56**, 15.10.1–15.10.18 (2016).
31. Van Loo, P. et al. Allele-specific copy number analysis of tumors. *Proc. Natl Acad. Sci. USA* **107**, 16910–16915 (2010).
32. Li, Y. et al. Constitutional and somatic rearrangement of chromosome 21 in acute lymphoblastic leukaemia. *Nature* **508**, 98–102 (2014).

Acknowledgements

We thank S. Dewhurst for insightful comments on this manuscript and N. Saini for generating the logo data. Research reported in this publication was supported by grants from the National Cancer Institute (no. R35CA210036), the Starr Cancer Consortium (grant no. 19-A9-047) and from the Breast Cancer Research Foundation to T.d.L. T.d.L. is an American Cancer Society Rose Zarucki Trust Research Professor. D.A.G. is supported by the National Institutes of Health Intramural Research Program Project (no. ZIAES103266). J.M. is supported by grants from the National Cancer Institute (no. R00CA212290), an MSK Cancer Center Support Grant/Core Grant (no. P30 CA008748), the Starr Cancer Consortium (grant no. 112-0030), the V Foundation for Cancer Research and a Pew Biomedical Scholar Fellowship.

Author contributions

J.M., T.d.L. and P.J.C. conceived and designed the study. J.M., A.C., A.D., K.C. and E.T. performed the experiments. J.M., A.C., D.A.G., L.J.K., P.J.C. and T.d.L. analyzed the data. J.M. and T.d.L. wrote the manuscript with contributions from P.J.C., A.C. and D.A.G. All authors approved the final manuscript.

Competing interests

T.d.L. is a member of the scientific advisory board of Calico Life Sciences. The other authors declare no competing interests.

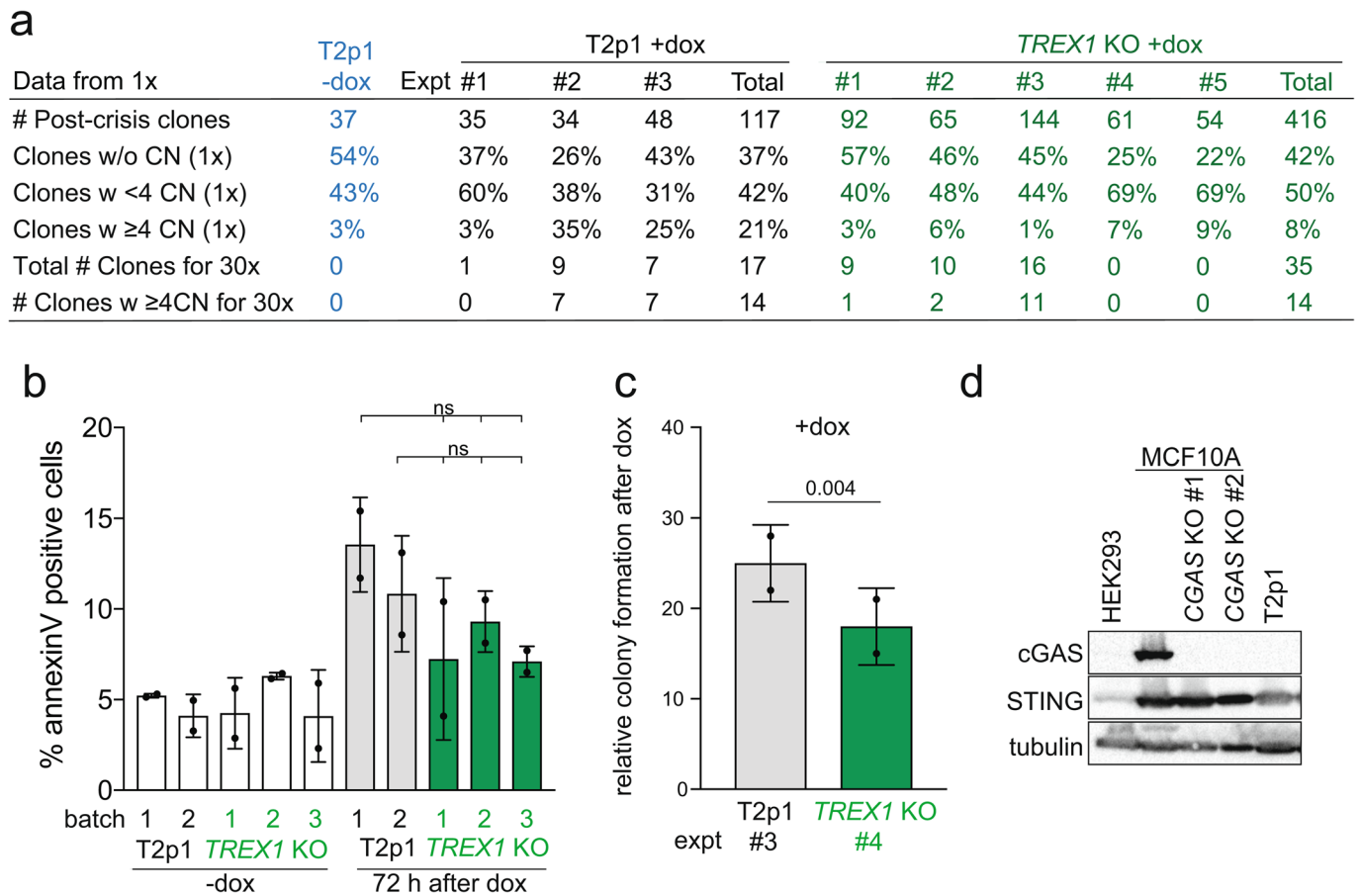
Additional information

Extended data is available for this paper at <https://doi.org/10.1038/s41588-020-0667-5>.

Supplementary information is available for this paper at <https://doi.org/10.1038/s41588-020-0667-5>.

Correspondence and requests for materials should be addressed to J.M., P.J.C. or T.d.

Reprints and permissions information is available at www.nature.com/reprints.

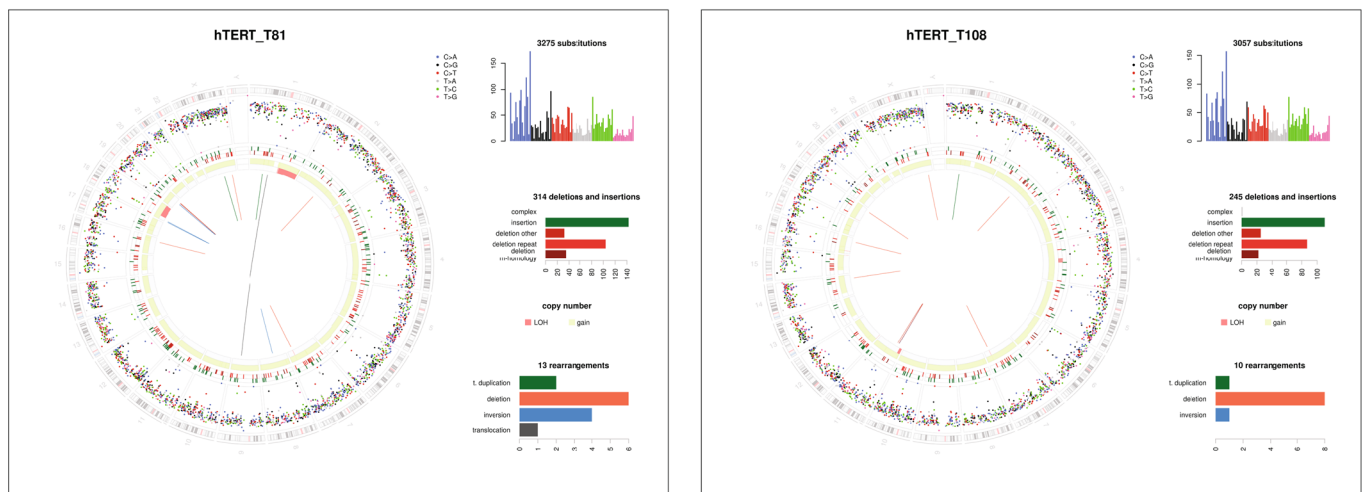


Extended Data Fig. 1 | TREX1 affects CN alterations but not cell viability after telomere crisis. **a**, Summary of the number of post-crisis T2p1 and *TREX1* KO clones analyzed from independent telomere crisis experiments, the frequency of simple and complex CN changes detected (1x) and the number of clones selected for 30x WGS. Note that many more *TREX1* KO than T2p1 clones were analyzed by 30x WGS. This does not reflect greater survival and does not introduce a bias. Uninduced T2p1 clones were not analyzed by 30x WGS since they were shown to lack chromothripsis previously (ref. 4). **b**, Plot showing percentage of annexin V positive cells 72 hours after dox treatment of two batches of T2p1 and three batches of *TREX1* KO lines. Bars represent mean and s.d. from $n=2$ independent experiments. P values derived from Student's t test. (ns: not significant). **c**, Plating efficiency of T2p1 and *TREX1* KO cells after dox induction. Cells were seeded in 96 well plates at different cell number per well and scored for positive wells two weeks later. Bars represent mean and s.d. from $n=3$ independent experiments. P values derived from Student's t test. The numbers below the graph refer to the experiments shown in (a). **d**, Immunoblot of the lack of cGAS protein in T2p1 cells. HEK293, MCF10A, MCF10A CGAS KO¹⁶ are shown for comparison. The protein STING is present in all cell lines.

a

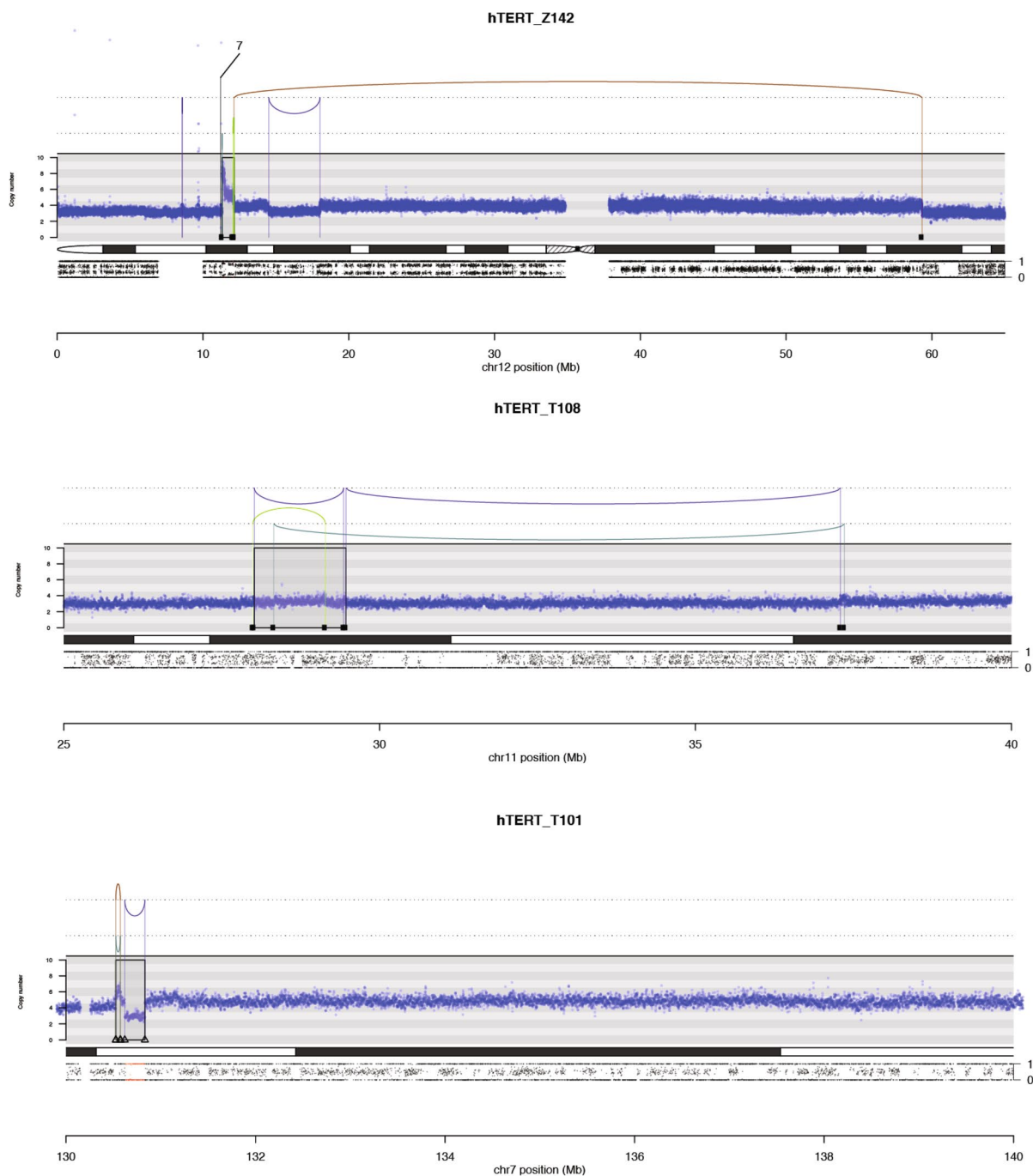


b

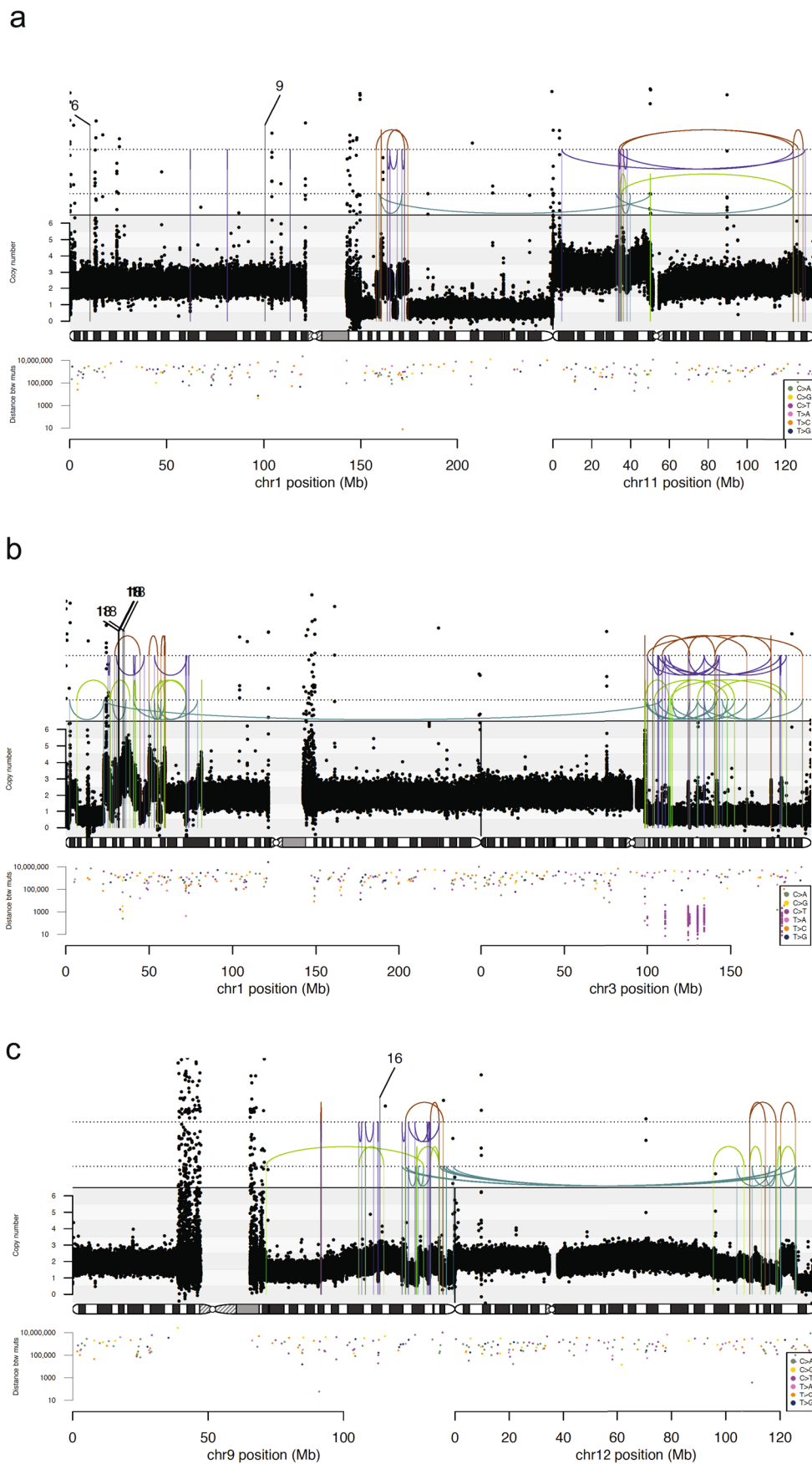


Extended Data Fig. 2 | See next page for caption.

Extended Data Fig. 2 | Circos plots of genome alterations in T2p1 post-crisis clones. a, Four T2p1 post-crisis clones with complex events identified by 1x WGS were analyzed by 30x WGS and their associated genome plots are shown. Circos plots show somatic mutations including substitutions (outermost, dots represent 6 mutation types: C>A, blue; C>G, black; C>T, red; T>A, grey; T>C, green; T>G, pink), indels (the second outer circle, color bars represent five types of indels: complex, grey; insertion, green; deletion other, red; repeat-mediated deletion, light red; microhomology-mediated deletion, dark red) and rearrangements (innermost, lines representing different types of rearrangements: tandem duplications, green; deletions, orange; inversions, blue; translocations: grey). The number of detected base substitutions, indels, and rearrangements are shown to the right of each panel. **b**, Genomic information on two post-crisis *TREX1* KO clones displayed as in (a).

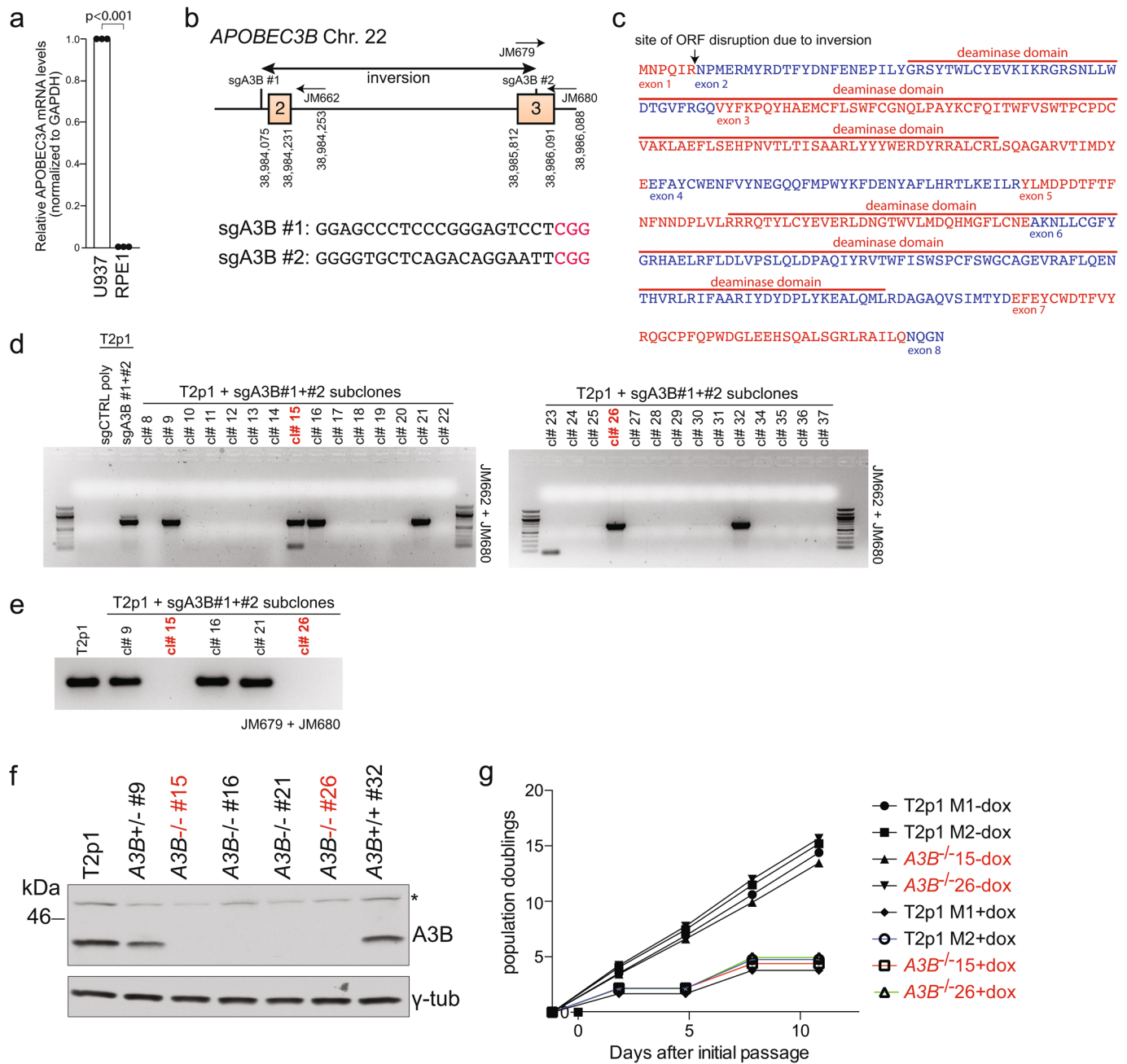


Extended Data Fig. 3 | Examples of chromothripsis-like and Local Jump events in *TREX1* KO post-crisis clones. Three *TREX1* KO post-crisis subclones with complex (Z142) events, simple (T108) events or no rearrangements (T101) identified by 1x WGS were analyzed by 30x WGS. DNA CN profiles and rearrangement joins were obtained from Battenberg analysis of 30x target coverage genomic sequencing data. Annotation as in Fig. 1a. Variant allele frequency tracks are shown below the chromosome ideograms. Examples show a chromothripsis-like event in Z142, a local n jump in T108, and a local 3 jump in T101.

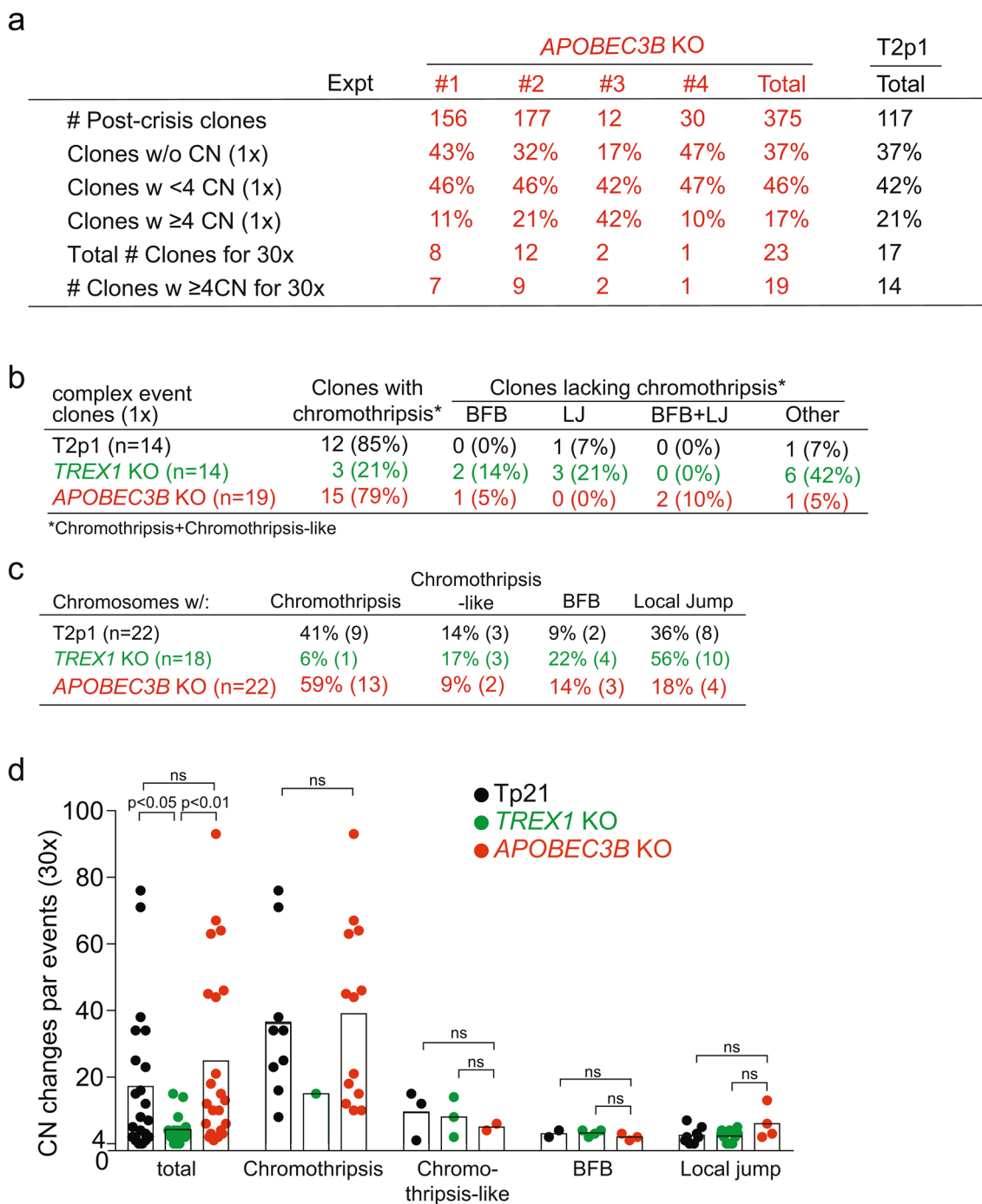


Extended Data Fig. 4 | See next page for caption.

Extended Data Fig. 4 | Clonal evolution in post-crisis clones M2dox120, A3B1590 and M2dox121. **a**, Chromothripsis and rainfall plot of clone M2dox120 involving chromosomes 1 and 3. **b**, Chromothripsis and rainfall plot of clone A3B1590 involving chromosomes 1 and 11. **c**, Chromothripsis and rainfall plot of clone M2dox121 involving chromosomes 9 and 12. Evidence of parallel crises manifested as chromothripsis affecting two distinct regions on separate chromosomes in (a) and (b). Evidence for sequential events affecting the same derivative chromosome in (c). Top of each plot: the arcs represent the two ends of rearrangements. Arcs are grouped from top to bottom by the type of rearrangement orientation as follows: deletion (D;+ -); tandem duplication (TD; -+); tail-tail (TT;++); head-head (HH; -). The bottom of each plot shows filled circles which represent positions of point mutations colored by mutation type. The Y-axis shows the distance of each mutation to the next on the same chromosome, with the respective axis on the left-hand side of the graph.



Extended Data Fig. 5 | Gene Editing of *APOBEC3B*. **a**, Relative *APOBEC3A* mRNA levels (normalized to *GAPDH*) in U937 and RPE1 cells determined by qRT-PCR showing that *APOBEC3A* is not expressed in the telomere crisis cell system. Bars represent mean and s.d. from $n=3$ independent experiments. **b**, Schematic of the *APOBEC3B* locus showing landmarks relevant to CRISPR editing. sgRNA sequences used for CRISPR editing are shown below. Protospacer adjacent motifs are marked in red. **c**, *APOBEC3B* amino acid sequence showing exon boundaries, catalytic domains, and predicted gene disruption from CRISPR editing. **d**, PCR screening identifies clones harboring at least one copy of a CRISPR-generated inversion in the *APOBEC3B* locus. Clones used for subsequent experiments are marked in red. **e**, PCR screening confirms allelic disruption of the endogenous *APOBEC3B* locus. Clones used for subsequent experiments are marked in red. **f**, Immunoblot for *APOBEC3B* and γ -tubulin shows absence of *APOBEC3B* in 4 CRISPR-edited clones. Clones #15 and #26 were selected for further study. Asterisk marks a cross-reacting polypeptide. Blot is representative of $n=3$ independent experiments. **g**, Proliferation of the *APOBEC3B* CRISPR KO clones with and without doxycycline induction of TRF2-DN. Data from $n=1$ experiment.



Extended Data Fig. 6 | 1x and 30x WGS information on *APOBEC3B* KO post-crisis clones. **a**, Summary of the number of *APOBEC3B* KO clones isolated from independent telomere crisis experiments, the frequency of simple and complex CN changes detected (1x) and the number of clones selected for 30x WGS. Parallel information on the T2p1 (Extended Data Fig. 1a) is provided for comparison. **b**, and **c**, Information of complex events in *APOBEC3B* KO clones as in Fig. 2b and Fig. 2c. Parallel information on T2p1 and *TREX1* KO post crisis clones is provided (from Fig. 2). **d**, Bar plot displaying the number of CN changes associated with the complex events indicated in *APOBEC3B* KO clones together with T2p1 and *TREX1* KO information (from Fig. 2d). P values derived from ANOVA (ns: not significant).